https://doi.org/10.1016/j.applthermaleng.2019.114070

Optical performance of parabolic trough solar collectors under condition of multiple optical factors

Bin Zou[a, b], Yiqiang Jiang[a, *], Yang Yao[a], Hongxing Yang[b]

[a] School of Architecture, Harbin Institute of Technology; Key Laboratory of Cold Region Urban and Rural Human Settlement Environment Science and Technology, Ministry of Industry and Information Technology, Harbin, China

[b] Renewable Energy Research Group (RERG), Department of Building Services Engineering, The Hong Kong Polytechnic University, Hong Kong, China

Abstract

Since various optical factors, including sunshape and optical errors, coexist in practice, their coupling effects on the PTC's optical performance deserve in-depth explorations. Previous studies mainly focused on individual effects of several typical optical errors or simple description of optical errors using a unified Gaussian model. Thus, this study is committed to investigating the coupling effects of multiple optical factors on the PTC's optical performance based on the theoretically individual characterization of each optical factor. The Monte Carlo Rays Tracing method was adopted, and the effective sunshape model was established for sampling of incident rays by convolving the incident sunshape model with the specularity error model. It is

revealed that larger circumsolar ratio and specularity error produced more uniform heat flux distribution on the absorber. The advantage of high optical quality reflectors in improving optical efficiency was more outstanding in clearer weather. As circumsolar ratio was more than 0.2, improving specular quality to very high degree (<3 mrad) reduced instead the optical efficiency. When tracking error and slope error were maintained respectively less than 4 mrad and 2 mrad, the weakening of optical efficiency was limited. The optical efficiency was more sensitive to slope error than to tracking error. The offset direction along positive Y-axis caused at maximum 2.19 times increase in heat flux density than that without optical errors, which causes threat of overheating to the absorber. When alignment error and tracking error were in the opposite direction, the optical loss could be compensated, whereas that in the same direction enlarged the optical loss. The slope error weakened the compensation effect and aggravated the weakening effect.

Keywords: Parabolic trough solar collector; Optical factors; Individual characterization; Coupling effects; Heat flux distribution; Optical efficiency

* Corresponding authors: School of Architecture, Harbin Institute of Technology; Key Laboratory of Cold Region Urban and Rural Human Settlement Environment Science and Technology, Ministry of Industry and Information Technology, Harbin, China

E-mail: jyq7245@163.com (Y. Jiang)

Nomenclature

a	offset angle (°)
A_i	area of the ith grid (m^2)
b_{sl}	slope error (mrad)
b_{tr}	tracking error (mrad)
CL	local concentration ratio
CL_i	local concentration ratio of the ith grid
d_a	out diameter of the absorber tube (m)
d_g	out diameter of the glass envelope (m)
f	focal length (m)
I_D	direct normal solar radiation intensity (W/m^2)
I_i	local energy flux density on the ith grid (W/m^2)
l_a	offset distance (m)
L_a	the length of the used PTC module (m)
N_n	the total number of grid divided on the absorber
W	aperture width (m)

Greek symbols

α_a	absorptance of the absorber
δ	radial angle of the solar disk (δ=4.65mrad)
δ_Δ	maximum radial angle of the Buie's model (δ_Δ=43.6mrad)
η_o	optical efficiency (%)
θ_s	radial angle of the point on the solar profile (mrad)
θ_{sp}	the deviation of the reflected beam from the specular direction (mrad)
ρ_r	reflectance of the parabolic reflector
σ_{sl}	standard deviation of slope error (mrad)
σ_{sp}	standard deviation of specularity error (mrad)
τ_g	transmittance of the glass envelope

φ_a	circumferential angle of the absorber (°)

Abbreviations

CSP	concentrating solar power
CSR	circumsolar ratio
CPEM	Change Photon Energy Method
FVM	Finite Volume Method
IMCRT	Inverse Monte Carlo Ray Tracing
IR	infrared radiation
MCM	Monte Carlo Method
MCRT	Monte Carlo Ray Tracing
PTC	parabolic trough solar collector
PSOA	particle swarm optimization algorithm
RTM	ray tracing method

1. Introduction

The parabolic trough solar collector (PTC) technology is currently the most cost-effective and developed technology in concentrating solar power (CSP) area [1-3]. Apart from power generation, PTCs have also been applied in many other fields, such as industrial process heat production, desalination, refrigeration and air-conditioning [4-9], showing great development prospects. As a typical kind of solar concentrator, a PTC module consists mainly of a parabolic reflector and a receiver tube that is installed at the focal line of the parabolic reflector, as shown in Fig. 1. The concentrating process of sunrays (i.e. optical performance) is critical to the overall performance of the PTC. In engineering practice, there are various optical

factors, such as uneven sunshape and optical errors including specularity error, tracking error, slope error and absorber alignment error, which have remarkable influences on the optical performance of the PTC. Thus, it is of great practical significance to study the coupling effects of multiple optical factors on the PTC's optical performance. In the past, researchers carried out plenty of optical investigations on the PTC from various aspects, some of them considering the optical factors and others not. The methods adopted to treat the optical factors in those studies changed from one to another. In order to fully introduce the research actuality of the optical performance of the PTC, a comprehensive review on the major researches in the field was conducted as follows.

The optical studies of the PTC date back to 1970s, during which theoretical analyses on the rays-concentrating properties of the PTCs were conducted [10, 11]. Several typical studies achieving substantial progress in research on PTC's optical performance were also conducted in 1980s [12-18]: Jeter [12-14] proposed an integral formula for calculating the energy flux based on analytical method. His results were usually used as references for optical model validation by other researchers [23-26, 36]. Guven and Bannerot [15, 16] clarified performance influencing factors and divided optical errors into two types: random and non-random. Bendt et al. [17] developed a Gaussian approximation model for defining each optical error. In their study, all the optical factors were described by Gaussian distribution, and the total optical error was expressed by the square root of the sum of the square of each optical

factor. The Gaussian model established by Bendt et al. [17] was also adopted for optical analyses in later studies [16, 18-20]. Since the analytical method struggled in complex system, the ray-tracing method (RTM) with high flexibility became more attractive [21, 22].

The advanced computer technology facilitated the optical simulation of solar concentrators in recent years. The studies involving PTC's optical performance conducted in recent ten years were summarized chronologically in Table 1.

1 Table 1 Review on studies involving PTC's optical performance

Literature	Method	Content focused	Optical factors mentioned
Grena et al. [23, 24]	RTM	Investigated the individual effects of tracking error, mirror imperfection, reflector deformation on PTC's optical performance. Discussed the efficiency improvement using IR-reflective film on the non-irradiated part of the receiver.	Tracking error was defined theoretically Mirror imperfection was treated as Gaussian model
He et al. [25]	MCRT, FVM	MCRT coupled with FVM was introduced. Discussed effects of geometric concentration ratio and rim angle on heat flux distribution.	None
Cheng et al. [26-30]	MCRT, FVM, PSOA	A unified MCRT code was developed. Studied effects of operational and geometrical parameters on performance. Compared the optical and thermal performance of different types of PTCs. Conducted optical optimization of PTC using PSOA.	None [26-28, 30] Tracking error and surface error were defined separately [29]
Huang et al. [31, 32]	Theoretical analysis	Analyzed error transfer from surface slope to reflected and refractive ray.	Slope error was defined as Gaussian model
Huang et al. [33]	Analytical and integral algorithm	Analytical equation for optical efficiency was derived. Effects of optical errors and material properties were investigated.	Optical errors were defined together as Gaussian model
Zhu et al. [34, 35]	Analytical method	A new algorithm for calculating intercept factor based on first-principle treatment to optical errors was proposed.	Slope error and absorber alignment error were defined theoretically Other errors were treated as Gaussian model
Hachicha et al. [36]	Numerical-geometrical method	Developed an optical-thermal model for calculating heat flux distribution on the absorber.	Two extra rays were used to represent effects of optical factors
Khanna et al. [37, 38]	Analytical method	Developed expressions for flux and temperature distribution on the bent	Optical errors were defined together as

		absorber.	Gaussian model
Wirz et al. [39]	MCRT, FVM	Explored efficiency-improvement potential by component idealizations and secondary optics	Dispersion error was defined as Gaussian model Buie'e sunshape
Xu et al. [40, 41]	Analytical and experiment	Investigated effects of end loss and its compensation measures.	None
Zhao et al. [42]	MCRT	Investigated effects of geometric ratio, rim angle and material properties on flux distribution on the absorber.	None
Rodriguez-Sanchez et al. [43]	Analytical method, RTM	Used a second-stage mirror to improve the concentration ratio.	None
Wang et al. [44]	MCRT	Explored effects of glass cover on flux distribution and optimization.	None
Zhao et al. [45]	MCRT	Investigated individual influences of installation and tracking errors on the optical performance.	Installation and tracking error were defined
Zhang et al. [46]	MCRT	Discussed influences of geometrical deformation on the optical performance.	Geometrical deformation was defined
Song et al. [47, 48]	Analytical and integral method	Developed a descending dimension algorithm for calculating flux distribution.	Buie's sunshape
Liang et al. [49, 50]	MCM, FVM, CPEM	Compared and optimized MCRT coupled with FVM for optical simulation.	Tracking and absorber alignment error were defined theoretically
Serrano-Aguilera et al. [51, 52]	IMCRT	Defined and modified reflector geometry using IMCRT	None
Mwesigye et al. [53]	MCRT	Explored individual influences of slope and specularity error on optical and thermal performance.	Slope and specularity error were treated as Gaussian model
Sun et al. [54]	Analytical method and experiment	Developed an optimized tracking strategy for double-axis PTC.	None

Song et al. [55]	RTM, FVM	Investigated individual influences of incident angle, tracking error, alignment error and direct incident radiation on the performance.	Tracking and absorber alignment error were defined theoretically
Zou et al. [56]	MCRT, theoretical analysis	Discussed effects of geometrical parameters on the optical performance.	None
Hoseinzadeh et al. [57]	MCM	Conducted geometric optimization of PTC using MCM	Optical errors were treated together as Gaussian model
Cheng et al. [58]	MCRT, PSOA	Proposed a computing method of long-time average optical efficiency fitting formulas.	Tracking and surface error were defined as Gaussian model
Fan et al. [59]	MCRT	Optimized the MCRT by increasing iterations to reduce computing cost.	None
Zou et al. [60]	Analytical and integral method	Developed a new simple algorithm for critical diameter and intercept under absorber alignment error.	Absorber alignment error was defined theoretically
Yilmaz et al. [61]	Summarization and analysis	A review: summarized optical and thermal modelling approaches and performance improvement techniques.	Cited from others literatures (Gaussian model)
Bellos et al. [62]	Summarization and analysis	A review: summarized optical and thermal modifications for PTC and suggested future trend.	None
Manikandan et al. [63]	Summarization and analysis	A review: summarized techniques for enhancing the optical and thermal efficiency of PTC.	None
Bellos et al. [64]	FEM	Installed a booster reflector at the end of the tough to enhance the optical performance under non-zero incident angle.	None

2 Note: “None” means that optical factors were not mentioned in the literature

From Table 1, it can be found that previous studies of the PTC's optical performance were mainly divided into three categories: parametrical analysis and optimization [25-30, 39, 42-44, 56, 57], algorithm development and improvement [31-38, 47-52, 54, 59-61], and investigations on individual effects of optical factors on the PTC's performance [23, 24, 40, 41, 45, 46, 53, 55]. As for parametrical analysis and optimization, researchers usually investigated the effects of geometrical parameters, such as aperture width, focal length, rim angle, geometrical concentration ratio, absorber diameter and glass diameter, on the PTC's performance, and then conducted corresponding optimizations. Most studies were conducted under ideal conditions (i.e. without optical errors) and several contained a synthetic optical error of unified Gaussian approximation. As for algorithm development and improvement, efforts were mainly made to develop a new time-saving algorithm or improve the MCRT for calculating the optical efficiency or heat flux distribution. Those studies have never discussed the coupling effects of optical factors. As for investigations on individual effects of optical factors on the PTC's performance, studies were focused on influences of certain single optical error, such as tracking error, surface error and alignment error, on the PTC's optical performance. In those studies, only the individual effects of several special optical errors were discussed separately without proper coupling with other factors. Moreover, the used sunshape was usually simplified as a uniform solar disk, which is impractical. Therefore, it can be found from the above literature that although numerous studies have been performed for

investigating the optical performance of the PTC, few explored comprehensively the coupling effects of multiple optical factors. The only way to combine the effects of all the optical factors together in the past was the unified Gaussian model proposed by Bendt et al. [17]. The Gaussian model adopted a total optical error expressed by the square root of the sum of the square of each optical factor to represent the combined effect of all the optical factors, which was just an approximation model. This model, in fact, cannot reflect the essence of each optical error and lose the geometrical and spatial dependence of some optical errors, such as slope error and absorber alignment error. Thus, it is theoretically necessary and more reasonable to characterize each optical factor separately according to their generation principles. Therefore, this paper aims to explore the coupling effects of multiple optical factors on the PTC's optical performance based on the theoretically individual characterization of each optical factor. The Buie's model [65] which was established based on the vast data collected by the Lawrence Berkeley Laboratories (LBL) and the German Aerospace Center (DLR) will be adopted to characterize the sunshape. All the optical errors will be defined individually based on their geometrical principles. The effective reflected sunshape model was established for sampling of incident sunrays by convolving the incident sunshape model with the specularity error model. The coupling effects of various optical factors on the PTC's optical performance will be investigated comprehensively using the MCRT.

2. Description of sunshape and optical errors

2.1 Effective sunshape

Due to the limb darkening and atmospheric attenuation scattering, the radiation intensity distribution on the solar image obtained on earth is uneven [66, 67]. As mentioned above, this study utilized the Buie's model as the original sunshape model. In Buie's model [65], the solar profile was divided into two parts: the solar disk with a radial angle of 4.65 mrad and the aureole (circumsolar region) which was produced by the scattering caused by the solar beam interacting with atmospheric particles. The most important parameter in the model is the circumsolar ratio (CSR) which is defined as the ratio of the energy contained within the circumsolar region (aureole) to the total energy contained in both the solar disk and aureole. Their model is given by Eq. (1) [65].

$$\phi(\theta_s)=\begin{cases}\dfrac{\cos(0.326\theta_s)}{\cos(0.308\theta_s)} & \theta_s \le 4.65\ \text{mrad}\\ e^{\kappa}\theta_s^{\gamma} & \theta_s > 4.65\ \text{mrad}\end{cases} \tag{1}$$

where θ_s is the radial angle of any point on the solar image, κ and γ are given by Eq. (2) and Eq. (3) respectively [65].

$$\kappa = 0.9\ln(13.5\chi)\chi^{-0.3} \tag{2}$$

$$\gamma = 2.2\ln(0.52\chi)\chi^{0.43} - 0.1 \tag{3}$$

where χ is the circumsolar ratio (i.e. CSR), and given by Eq. (4) [65].

$$\chi = \frac{2\pi\int_{\delta}^{\delta_\Delta}\phi(\theta_s)\sin(\theta_s)d\theta_s}{2\pi\int_{0}^{\delta_\Delta}\phi(\theta_s)\sin(\theta_s)d\theta_s} \tag{4}$$

where δ and δ_{Δ} are the radial angular size of the solar disk (δ=4.65 mrad) and the upper limit of the circumsolar region (δ_{Δ} = 43.6 mrad) respectively.

In actual system, because of the imperfect microscopic texture of the reflector, the non-specular reflection occurs, which was defined as the specularity error. According to literatures [68-70], the Gaussian distribution was proved to be feasible and reliable to characterize the specularity error. Thus, the probability density function of specularity error is given by Eq. (5).

$$R(\theta_{sp}) = \frac{1}{\sqrt{2\pi}\sigma_{sp}} \exp\left(-\frac{\theta_{sp}^2}{2\sigma_{sp}^2}\right) \tag{5}$$

As Fig. 2 shows, due to the diffusing effect of the specularity error, the sunrays in the reflected optical cone will be redistributed. Therefore, the reflected sunshape need to be remodeled. According to mathematical theory, the effective sunshape model after reflection can be expressed by convolving the original sunshape model (i.e. Eq. (1)) with the specularity error model (i.e. Eq. (5)), and given by Eq. (6).

$$\phi_{eff}(\theta_s) = \int_{-\delta_{\Delta}}^{\delta_{\Delta}} \phi(\theta') R(\theta_s - \theta') d\theta' \tag{6}$$

Obviously, the effects of the effective sunshape on the PTC's performance depend both on the original incident solar profile (CSR) and the specularity error (σ_{sp}), which will be discussed in detail in section 4.

2.2 Optical errors

Tracking error (b_{tr}) is the angle between the plane containing the vertex and focal line of the collector and the plane containing the focal line and the sun. It is determined by the accuracy of the tracking system and remains unchanged for all the

points on the reflector. Thus, the same tracking error can be applied for all points on the reflector.

Slope error (b_{sl}) is the angular deviation of the actual surface normal direction from the ideal normal direction. Note that an angular deviation of the surface normal vector causes twice the angular deviation of the reflected rays. Since no measured data can be used, the slope error used in this study was generated by Gaussian model [17], which is given by Eq. (7).

$$R(b_{sl}) = \frac{1}{\sqrt{2\pi}\sigma_{sl}} \exp\left(-\frac{b_{sl}^2}{2\sigma_{sl}^2}\right) \tag{7}$$

Absorber alignment error is defined as the installation deviation of the absorber tube from the focal line of the parabolic reflector. It is specified by two parameters: the offset distance (l_a) and the offset angle (a). For more clarity, the geometric description of each optical error is shown in Fig. 3. In the figure, ∠B'AC' is the actual reflected optical cone caused by the optical errors and ∠BAC is the reflected optical cone under ideal conditions (without optical errors).

3. MCRT and parameter definition

3.1 MCRT model and validation

Monte Carlo Ray Tracing (MCRT) method is a powerful tool for simulating the optical performance of the PTC. The basic idea of MCRT is as follows: Firstly, the position and direction of the incident rays coming from the sun are initialized according to the original sunshape model. And then, the optical behaviors, such as reflection, transmission, absorption, on each interface are determined by a series of

uniformly generated random numbers, and the propagating path of each ray is traced accordingly. Finally, the landing positions of the rays on the outer surface of the absorber tube are recorded and used to produce the statistical results of the flux distribution. For detailed information about MCRT, please refer to the authors' previous study [56].

The developed MCRT model was validated against the results presented in literatures [12, 36, 48] which adopted respectively analytical method, geometrical-numerical method and descending dimension integral algorithm for the same PTC module. The radial angle of the incident solar disk used was 7.5 mrad [12]. The major parameters of the PTC module used for model validation were as follows [12]: the aperture width was 4.4 m, the focal length was 1.1 m, the absorber diameter was 0.07 mm, the reflectance, transmittance and absorptance were all equal to 1. The results of the local concentration ratio (*CL*) distribution are presented in Fig. 4. It can be clearly seen from the figure that the results obtained using the developed MCRT model agreed very well with that obtained presented in the literatures, which indicates that the four methods can be mutually validated.

3.2 Parameter definition

The local concentration ratio (CL_i) is defined as the ratio of local heat flux density (I_i) on the absorber surface to the incident solar radiation intensity (I_D) on the reflector aperture, and can be given by Eq. (8).

$$CL_i = \frac{I_i}{I_D} \tag{8}$$

The optical efficiency (η_o) is defined as the ratio of absorbed energy to the total energy incident on the aperture and calculated by Eq. (9).

$$\eta_o = \frac{\sum_{i=1}^{N_n} I_i \cdot A_i}{I_D \cdot W \cdot L_a} \tag{9}$$

4. Results and discussion

The current work adopted the SEGS LS-2 PTC module, which had been tested in Sandia National Laboratory, as the research prototype, the specifications of which are listed in Table 2 [71].

Table 2 Parameters of SEGS LS-2 PTC module [71]

Parameter	Value	Unit
W	5	m
f	1.84	m
L_a	7.8	m
d_a	0.07	m
d_g	0.115	m
α_a	0.96	——
ρ_r	0.93	——
τ_g	0.95	——

4.1 Effects of the effective sunshape

4.1.1 Effects on the distribution of local concentration ratio

Fig. 5 shows the effects of circumsolar ratio (CSR) on the distribution of local concentration ratio (*CL*) in the case of σ_{sp}=3 mrad. It can be seen from the figure that the angle span that receives the reflected rays (i.e. high flux area) increased and

the maximum *CL* decreased with the increase of CSR, indicating that more uniform heat flux distribution was produced by larger CSR. This is because more solar energy will be distributed in the circumsolar area and the radiation intensity at the central region of the solar disk is reduced as the CSR increases, producing more uniform incident solar radiation distribution. From the figure, we can also find that all the curves were symmetrical about φ_a=0°, and the double peaks of the curves were gradually transformed to the single peak with further increase of CSR.

Fig. 6 depicts the effects of specularity error (σ_{sp}) on the distribution of local concentration ratio (*CL*) in the case of CSR=0.1. It can be seen from the figure that with the increase of σ_{sp}, the distribution curve of *CL* became more homogenous, showing more uniform flux distribution on the absorber surface. The reason is that larger specularity errors scatter more reflected rays to a larger angle span in the reflected optical cone, producing a more uniform reflected sunshape. It can also be seen from Fig. 6 that in the high heat flux area of the absorber tube, a part of the heat flux was reduced and the other was increased with the increase of σ_{sp}. For example, when σ_{sp} was 5 mrad, the heat flux in the circumferential angle range between -75° and -25° (also between 25° and 75°) was smaller than that obtained for σ_{sp}=1 mrad, whereas the heat flux in the range between -25° and 25° was larger than that for σ_{sp} =1 mrad. This indicates that the specularity error plays a role of cutting peaks and filling valleys in the high heat flux area.

4.1.2 Coupling effects on the optical efficiency

Fig. 7 shows the variation of the optical efficiency (η_o) with circumsolar ratio (CSR) under different specularity errors (σ_{sp}). It can be observed from the figure that η_o declined consistently with the increase of CSR for all the specularity errors discussed. This is because with the increase of CSR, more solar radiation energy is distributed in the circumsolar area, causing more sunrays escaping from the PTC system (i.e. intercept factor reduced) and hence leading to larger optical loss. Taking σ_{sp}=1 mrad as an example, as the CSR rose from 0 to 0.5, the η_o decreased from 84.81% to 77.51%, dropping by 7.3%. It can also be found from Fig. 7 that the optical efficiency curves for two different specularity errors usually intersected at a certain CSR. When the CSR varied within a range less than the intersection point, the η_o for smaller σ_{sp} was larger than the η_o for larger σ_{sp}. Whereas, if the CSR increased beyond the intersection point, the η_o for smaller σ_{sp} would be smaller than the η_o for larger σ_{sp}. For example, the optical efficiency curves for σ_{sp}=1 mrad and σ_{sp} =7 mrad intersected at CSR=0.47. When the CSR was less than 0.47, the optical efficiency for σ_{sp}=1 mrad was larger than that for σ_{sp}=7 mrad, whereas it was smaller as the CSR was larger than 0.47. This indicates that when the weather is not good enough (i.e. CSR is large), reflectors with poorer specular quality (i.e. σ_{sp} is large) may produce lager efficiency. The reason is that when CSR is large enough, more energy is distributed in the peripheral area of the solar disk, and larger specularity errors scatter more peripheral radiation to the center area than smaller ones. Meanwhile, although part of the original central energy of the solar disk is dispersed

to a larger radial angle range, the relatively large acceptance angle of the absorber tube can still receive most of those dispersed sunrays. This is exactly the effect of cutting peaks and filling valleys of the specularity error in the high flux area, which was presented in Fig. 6. Therefore, with larger CSRs, larger specularity errors distribute more energy in an angle range that can be intercepted by the absorber under, producing higher efficiency. It can also be found from Fig. 7 that the intersection point between the efficiency curve for σ_{sp}=1 mrad and other curves increased with the increase of σ_{sp}. The intersection point between the curve for σ_{sp}=1 mrad with σ_{sp} =3 mrad, σ_{sp}=5 mrad, σ_{sp}=7 mrad and σ_{sp}=9 mrad was CSR=0.02, CSR=0.08, CSR=0.47, and more than 0.9, respectively. This demonstrates that the reflectors with high optical quality have less or even no advantage in improving the optical efficiency in bad weather.

Fig. 8 shows the variation of the optical efficiency (η_o) with specularity error (σ_{sp}) under different circumsolar ratios (CSR). It is easily seen from the figure that η_o increased slowly firstly when σ_{sp} was small and then dropped quickly with further increasing σ_{sp} for all the discussed CSRs. When σ_{sp} was small (less than 6 mrad), the optical efficiency differences between different CSRs were obvious, and became smaller and smaller with increasing σ_{sp} continuously. This demonstrates that the effects of CSR dominate when σ_{sp} is small and become less obvious as σ_{sp} increases to a large value range. From the figure, it can be found that the specularity error producing the highest efficiency for CSR=0.1, CSR=0.2, CSR=0.3, CSR=0.4

and CSR=0.35 was 3 mrad, 3.5mrad, 4 mrad, 4.5mrad and 5 mrad respectively. This demonstrates again that the advantage of the high quality reflector is more obvious in better weather. Therefore, the optical quality of the reflector used in sites with excellent solar resource should be as good as possible. Whereas, for the places with relatively high atmospheric turbidity (CSR is usually more than 0.2), it is not necessary to improve the specular quality of the reflector to a very high degree (σ_{sp} <3 mrad). Because almost no improvement or even small reduction of optical efficiency will be caused by reflectors with specularity error less 3 mrad in that cases, whereas the costs of those high quality mirrors are remarkable.

4.2 Effects of optical errors

This section discussed the effects of three main optical errors, including tracking error, slope error and absorber alignment error, on the optical performance of the PTC. The study was conducted with the effective sunshape of CSR=0.1 and σ_{sp} =4 mrad.

4.2.1 Effects on the distribution of local concentration ratio

Fig. 9 shows the effects of tracking error (b_{tr}) on the distribution of local concentration ratio (*CL*). It is clearly seen from the figure that the *CL* curves moved toward the right side of φ_a =0° which is the opposite side of the tracking error (left side shown in Fig. 3). This indicates that the tracking error (b_{tr}) destroys the symmetry of the *CL* distribution and more energy will be reflected to the opposite direction of the tracking error. It can also be found the figure that the peak *CL* increased slightly firstly with b_{tr} increasing from 0 mrad to 5 mrad and then

223 decreased obviously with b_{tr} further rising to 15 mrad. The left peak was always
224 larger than the right one. This indicates that as the tracking error vary in a range of
225 small values (< 5 mrad), the peak heat flux on the same side of the tracking error will
226 be enhanced, while that on the opposite side will be weakened. When b_{tr} was larger
227 than 7 mrad, the double peaks of *CL* curves were transformed to the single peak, and
228 the circle angle (φ_a) corresponding to the peak *CL* moved gradually to the right (i.e.
229 the opposite side of the tracking error).

230 Fig. 10 displays the effects of slope error (σ_{sl}) on the distribution of local
231 concentration ratio (*CL*). Because of the symmetry of Gaussian distribution, the *CL*
232 curves maintained symmetrical about φ_a=0° for any slope errors, as shown in Fig. 10.
233 The double peaks of the *CL* curves were transformed to the single peak when σ_{sl}
234 was more than 2.5 mrad. The peak *CL* decreased and the angle span of the high heat
235 flux increased with the increase of σ_{sl}. This means that the slope error (σ_{sl}) flattens
236 the *CL* curves and produces more uniform energy distribution on the absorber surface.

237 Fig. 11 shows the effects of the absorber alignment error on the distribution of
238 local concentration ratio (*CL*). Fig. 11(a) shows the results under different offset
239 distances (l_a) in the case of a=0° (i.e. the positive direction of X-axis). It can be seen
240 from the figure that when l_a was more than zero, the *CL* curves moved toward the
241 left side of φ_a=0° which is the opposite side of the offset direction (a=0°). This
242 indicates that more energy is distributed on the opposite side of the offset direction.
243 Fig. 11(a) also shows that when the l_a was within the range between 0.01 m and 0.03

m, there was only one peak for the *CL* curves. As the l_a increased more than 0.04 m, two peaks with different concentration ratios occurred. It can be expected that when l_a increased to a certain degree, the minimum *CL* between those two peaks will be zero. Fig. 11(b) shows the results under different offset distances (l_a) in the case of a =90° (i.e. the positive direction of Y-axis). It can be obviously seen from the figure that the offset direction along the Y-axis did not change the symmetry of the circumferential heat flux distribution on the absorber surface. It can also be clearly found that the high heat flux area shrank consistently and the *CL* curves became steeper with the increase of l_a. The two peaks of the *CL* curves were changed to one peak when l_a was more than 0.01 m. The peak *CL* increased sharply firstly and then declined quickly with the increase of l_a. The maximum *CL* in ideal case (l_a=0 m) was only 47.5, whereas the maximum *CL* obtained in the case of l_a=0.03 m was 104 which is almost 2.19 times that obtained in ideal case. This demonstrates that the offset direction along positive Y-axis may result in overheating on the absorber tube surface, which threatens the safety of the PTC system significantly and hence should be avoided in engineering practice.

4.2.2 Coupling effects on the optical efficiency

The coupling effects of tracking error (b_{tr}) and slope error (σ_{sl}) on the optical efficiency (η_o) were displayed in Fig. 12 and Fig. 13. Fig. 12 shows the variation of the optical efficiency (η_o) with tracking error (b_{tr}) under different slope errors (σ_{sl}). It shows clearly that η_o dropped constantly with the increase of b_{tr} under all the

discussed σ_{sl}. The downtrend of the optical efficiency curves became gentler with increasing σ_{sl}. Generally, when b_{tr} varied in a range of small values, the η_o dropped slightly, indicating that there is a small tracking error threshold within which the PTC maintains a relatively high efficiency. For example, when b_{tr} increased from 0 mrad to 4 mrad, the η_o under the condition of σ_{sl} =0 mrad decreased from 83.6% to 82.6%, dropping just by 1%. Therefore, in practice, the accuracy of the tracking system should be less than the threshold of the tracking error to achieve high performance for the PTC. From Fig. 12, it can also be observed that when σ_{sl} was less than 6 mrad, all of the optical efficiency curves intersected at b_{tr} =17 mrad after which the optical efficiencies for larger σ_{sl} were larger than the optical efficiencies for smaller σ_{sl}. This indicates that larger slope errors can to some extent compensate the optical loss caused by larger tracking errors. Fig. 13 shows the variation of the optical efficiency (η_o) with slope error (σ_{sl}) under different tracking errors (b_{tr}). Obviously, η_o decreased consistently with the increase of σ_{sl}. There is also a small range of σ_{sl} during which the η_o maintains at a relatively high level. For example, when σ_{sl} was less than 2 mrad, the η_o under the condition of b_{tr} =0 mrad was kept more than 82.36%. It can also be found from Fig. 14 that the optical efficiency difference between any two b_{tr} became smaller with the increase of σ_{sl}. This demonstrates that large slope errors, compared with the tracking error, have dominant influences on the optical efficiency. Comparing Fig. 12 and Fig. 13, it can be found that the optical efficiency (η_o) was more sensitive to the slope error (σ_{sl}) than to the

286 tracking error (b_{tr}). For example, when b_{tr} increased from 0 mrad to 8 mrad, the η_o
287 for σ_{sl} =0 mrad decreased from 83.6% to 77.9%, dropping only by 5.7%. Whereas,
288 when σ_{sl} increased from 0mrad to 8 mrad, the η_o for b_{tr} =0 mrad declined
289 remarkably from 83.6% to 57%, dropping by 26.6% which was much larger than the
290 former (5.7%). The reason is that an angular deviation of the surface normal vector
291 causes twice the angular deviation of the reflected rays (as shown in Fig. 3), which
292 leads to greater sensitivity of the optical efficiency (η_o) to the slope error (σ_{sl}).
293 Therefore, improving the local topography of the reflector surface is an effective way
294 to improve the PTC's performance.

295 Fig. 14 shows the coupling effects of absorber alignment error and tracking error
296 (b_{tr}) on the optical efficiency (η_o) under the condition of σ_{sl} =3 mrad. It is easily
297 seen from the figure that when b_{tr} is zero, the optical efficiency curve was
298 symmetrical about a =90°. An important fact found in Fig. 14 was that the optical
299 efficiencies (η_o) at a =0° under the condition of non-zero tracking error (b_{tr} ≠0) were
300 always larger than that under the condition of no tracking error (b_{tr} =0). Whereas the
301 optical efficiencies (η_o) at a =180° under the condition of non-zero tracking error
302 (b_{tr} ≠0) were smaller than that under the condition of no tracking error (b_{tr} =0). For
303 example, the η_o at a =0° for l_a =0.03 m in the case of b_{tr} =10 mrad was about
304 77.96%, larger than the η_o which was about 62.83% in the case of b_{tr} =0 mrad.
305 Whereas, the η_o at a =180° for l_a =0.03 m in the case of b_{tr} =10 mrad was just
306 26.67% which was much smaller than the η_o (62.83%) obtained without tracking

error. From Fig. 3, it is easily found that a=0° is in the opposite direction of the tracking error (b_{tr}) and a=180° is in the same direction. Therefore, it can be concluded from the above findings that when the absorber alignment error and the tracking error are in the opposite direction, the optical loss can to some extent be compensated by themselves, defined as compensation effect, whereas if those two errors are in the same direction, the optical loss will be enlarged, defined as weakening effect.

Fig. 15 shows the coupling effects of absorber alignment error and slope error (σ_{sl}) on the optical efficiency (η_o) under the condition of b_{tr}=5 mrad. Obviously, due to the coupling effects (i.e. compensation effect or weakening effect) of absorber alignment error and tracking error, the η_o for a=0° were larger than the η_o for a =180°. It can also be found from the figure that σ_{sl} weakened the compensation effect and aggravated the weakening effect. Moreover, the extent to which the slope error (σ_{sl}) reduced the compensation effect was greater than the extent to which the slope error (σ_{sl}) aggravated the weakening effect. For example, when σ_{sl} increased from 1 mrad to 9 mrad, the η_o for a=0° was reduced from 79.84% to 50.06%, dropping by 29.78%. Whereas, the η_o for a=180° was reduced from 45.96% to 39.78%, dropping only by 6.18% with σ_{sl} increased from 1mrad to 9mrad as well.

5. Conclusions

Due to coexistence of various optical factors, such as uneven sunshape and optical errors including specularity error, tracking error, slope error and absorber

alignment error, the PTC's practical performance depends greatly on their coupling effects. This study investigated comprehensively the coupling effects of multiple optical factors on the PTC's optical performance based on theoretically individual characterization of each optical factor. An effective sunshape model was established for sampling of incident sunrays by convolving the original sunshape model with the specularity error model. The MCRT method was adopted for the optical simulation, and some important findings were summarized as follows:

(1) Both larger CSRs and larger specularity errors produce more uniform heat flux distribution around the absorber surface. Small specularity errors (< 5 mrad) play the role of cutting peaks and filling valleys in the high heat flux area. The weakening effect of CSR on the optical efficiency becomes less obvious with increasing specularity error. The advantage of the high optical quality reflector is more outstanding in clearer weather. For the sites with relatively high atmospheric turbidity (CSR>0.2), high quality reflector (σ_{sp} <3 mrad) achieves little improvement or even cause small reduction of optical efficiency.

(2) More energy is distributed on the absorber part that is on the opposite side of the tracking error. The slope error flattens the curves of local concentration ratio and produces more uniform heat flux distribution. When the offset direction is in the positive Y-axis direction (i.e. a =90°), the peak local concentration ratio is 2.19 times that obtained without any optical errors, posing threat of overheating on the absorber surface, which should be avoided in engineering practice.

(3) The downtrend of the optical efficiency with tracking error becomes gentler with increasing slope error. Both the tracking error and the slope error should be less than a threshold (4 mrad and 2 mrad respectively) to achieve high optical efficiency. When the tracking error is larger than a certain value (>17 mrad), the larger slope errors can to some extent compensate the optical loss caused by the tracking error. The optical efficiency is more sensitive to the slope error than to the tracking error. Therefore, improving the local topography of the reflector surface is an effective way to enhance the PTC's performance.

(4) When the absorber alignment error and the tracking error are in the opposite direction, the optical loss can to some extent be compensated by themselves, defined as compensation effect, whereas that in the same direction will aggravate the optical loss, defined as weakening effect. The slope error weakens the compensation effect and aggravates the weakening effect. Moreover, the extent to which the slope error reduces the compensation effect is greater than the extent to which the slope error aggravates the weakening effect.

Acknowledgements

This work was supported by the National Key R&D Program of China (Project Number: 2017YF0702604).

References

[1] W. Schiel, Collector development for solar parabolic trough power plants, Bautechnik 89 (2012) 182-191.

[2] X.H. Xu, K. Vignarooban, B. Xu, K. Hsu, et al., Prospects and problems of concentrating solar power technologies for power generation in the desert regions, Renewable and Sustainable Energy Reviews 53 (2016) 1106-1131.

[3] F.Q. Wang, Z.M. Cheng, J.Y. Tan, Y. Yuan, et al., Progress in concentrated solar power technology with parabolic trough collector system: A comprehensive review, Renewable and Sustainable Energy Reviews 79 (2017) 1314-1328.

[4] S. Kalogirou, Use of parabolic trough solar energy collectors for sea-water desalination, Applied Energy 60 (1998) 65-88.

[5] S. Kalogirou, Parabolic trough collectors for industrial process heat in Cyprus, Energy 27 (2002) 813-830.

[6] A. Scrivani, T.E. Asmar, U. Bardi, Solar trough concentration for fresh water production and waste treatment, Desalination 206 (2007) 485-493.

[7] G.A. Fernandez, E. Zarza, L. Valenzuela, M. Perez, Parabolic-trough solar collectors and their applications, Renewable and Sustainable Energy Reviews 14 (2010) 1695-1721.

[8] P. Bermejo, F.J. Pino, F. Rosa, Solar absorption cooling plant in Seville, Solar Energy 84 (2010) 1503-1512.

[9] F.J. Cabrera, A. Fernandez-Garcia, R.M.P. Silva, M. Perez-Garcia, Use of parabolic trough solar collectors for solar refrigeration and air-conditioning applications, Renewable and Sustainable Energy Reviews 20 (2013) 103-118.

[10] K.E. Hassan, M.F. El-Refaie, Theoretical performance of cylindrical parabolic

391 solar concentrators, Solar Energy 15 (1973) 219-244.
392 [11] D.L. Evans, On the performance of cylindrical parabolic solar concentrators with
393 flat absorbers, Solar Energy 19 (1977) 379-385.
394 [12] S.M. Jeter, The distribution of concentrated solar radiation in paraboloid
395 collectors, Journal of Solar Energy Engineering 108 (1986) 219-225.
396 [13] S.M. Jeter, Calculation of the concentrated flux density distribution in parabolic
397 trough collectors by a semifinite formulation, Solar Energy 37 (1986) 335-345.
398 [14] S.M. Jeter, Analytical determination of the optical performance of practical
399 parabolic trough collectors from design data, Solar Energy 39 (1987) 11-21.
400 [15] H.M. Guven, R.B. Bannerot, Derivation of universal error parameters for
401 comprehensive optical analysis of parabolic troughs, Journal of Solar Energy
402 Engineering 108 (1986) 275-281.
403 [16] H.M. Guven, R.B. Bannerot, Determination of error tolerances for the optical
404 design of parabolic troughs for developing countries, Solar Energy 36 (1986)
405 535-550.
406 [17] P. Bendt, A. Rabl, H.W. Gaul, K.A. Reed, Optical analysis and optimization of
407 line focus solar collector, Paper No. SERI / TR-34-092, SERI, Golden, CO, 1979.
408 [18] G. Treadwell, N. Grandjean, Systematic rotation and receiver location error
409 effects on parabolic trough annual performance, Journal of Solar Energy
410 Engineering 104 (1982) 345-348.
411 [19] A. Rabl, P. Bendt, H. Gaul, Optimization of parabolic trough solar collectors,

412 Solar Energy 29 (1982) 407-417.
413 [20] A. Thomas, H.M. Guven, Effect of optical errors on flux distribution around the
414 absorber tube of a parabolic trough concentrator, Energy Conversion and
415 Management 35 (1994) 575-582.
416 [21] C. Saltiel, M. Sokolov, Optical analysis of solar energy tubular absorbers,
417 Applied Optic 21 (1982) 4033-4039.
418 [22] D. Prapas, B. Norton, S. Probert, Optics of parabolic-trough, solar-energy
419 collectors, possessing small concentration ratios, Solar Energy 39 (1987) 541-550.
420 [23] R. Grena, Optical simulation of a parabolic solar trough collector, International
421 Journal of Sustainable Energy 29 (2010) 19-36.
422 [24] R. Grena, Efficiency Gain of a solar trough collector due to an ir-reflective film
423 on the non-irradiated part of the receiver, International Journal of Green Energy 8
424 (2011) 715-733.
425 [25] Y.L. He, J. Xiao, Z.D. Cheng, Y.B. Tao, A MCRT and FVM coupled simulation
426 method for energy conversion process in parabolic trough solar collector,
427 Renewable Energy 36 (2011) 976-85.
428 [26] Z.D. Cheng, Y.L. He, F.Q. Cui, R.J. Xu, Y.B. Tao, Numerical simulation of a
429 parabolic trough solar collector with nonuniform solar flux conditions by coupling
430 FVM and MCRT method, Solar Energy 86 (2012) 1770-1784.
431 [27] Z.D. Cheng, Y.L. He, F.Q. Cui, A new modelling method and unified code with
432 MCRT for concentrating solar collectors and its applications, Applied Energy 101

(2013) 686-698.

[28] Z.D. Cheng, Y.L. He, K. Wang, B.C. Du, F.Q. Cui, A detailed parameter study on the comprehensive characteristics and performance of a parabolic trough solar collector system, Applied Thermal Engineering 63 (2014) 278-289.

[29] Z.D. Cheng, Y.L. He, F.Q. Cui, B.C. Du, Z.J. Zheng, Y. Xu, Comparative and sensitive analysis for parabolic trough solar collectors with a detailed Monte Carlo ray-tracing optical model, Applied Energy 115 (2014) 559-572.

[30] Z.D. Cheng, Y.L. He, B.C. Du, K. Wang, Q. Liang, Geometric optimization on optical performance of parabolic trough solar collector systems using particle swarm optimization algorithm, Applied Energy 148 (2015) 582-593.

[31] W.D. Huang, Z.F. Han, Theoretical analysis of error transfer from the surface slope to the reflected ray and their application in the solar concentrated collector, Solar Energy 86 (2012) 2592-2599.

[32] W.D. Huang, Y.P. Li, Z.F. Han, Theoretical analysis of error transfer from surface slope to refractive ray and their application to the solar concentrated collector, Renewable Energy 57 (2013) 562-569.

[33] W.D. Huang, P. Hu, Z.H. Chen, Performance simulation of a parabolic trough solar collector, Solar Energy 86 (2012) 746-755.

[34] G.D. Zhu, A. Lewandowski, A new optical evaluation approach for parabolic trough collectors: first-principle optical intercept calculation, Journal of Solar Energy Engineering 134 (2012) 041005-1-8.

[35] M. Binotti, G.D. Zhu, A. Gray, G. Manzolini, P. Silva, Geometric analysis of three-dimensional effects of parabolic trough collectors, Solar Energy, 88 (2013) 88-96.

[36] A.A. Hachicha, I. Rodriguez, R. Capdevila, A. Oliva, Heat transfer analysis and numerical simulation of a parabolic trough solar collector, Applied Energy, 111 (2013) 581-592.

[37] S. Khanna, S.B. Kedare, S. Singh, Analytical expression for circumferential and axial distribution of absorbed flux on a bent absorber tube of solar parabolic trough concentrator, Solar Energy 92 (2013) 26-40.

[38] S. Khanna, S. Singh, S.B. Kedare, Explicit expressions for temperature distribution and deflection in absorber tube of solar parabolic trough concentrator, Solar Energy 114 (2015) 289-302.

[39] M. Wirz, J. Petit, A. Haselbacher, A. Steinfeld, Potential improvements in the optical and thermal efficiencies of parabolic trough concentrators, Solar Energy 107 (2014) 398-414.

[40] C.M. Xu, Z.P. Chen, M. Li, P. Zhang, X. Ji, X. Luo, et al., Research on the compensation of the end loss effect for parabolic trough solar collectors, Applied Energy 115 (2014) 128-139.

[41] M. Li, C.M. Xu, X. Ji, P. Zhang, Q.F. Yu, A new study on the end loss effect for parabolic trough solar collectors, Energy 82 (2015) 382-394.

[42] D. Zhao, E. Xu, Q. Yu, D. Lei, The simulation model of flux density distribution

475 on an absorber tube, Energy Procedia 69 (2015) 250-258.
476 [43] D. Rodriguez-Sanchez, Gary. Rosengarten, Improving the concentration ratio of
477 parabolic troughs using a second-stage flat mirror, Applied Energy 159 (2015)
478 620-632.
479 [44] F.Q. Wang, J.Y. Tian, L.X. Ma, C.C. Wang, Effects of glass cover on heat flux
480 distribution for tube receiver with parabolic trough collector system, Energy
481 Conversion and Management 90 (2015) 47-52.
482 [45] D.M. Zhao, E.S. Xu, Z.F. Wang, Q. Yu, L. Xu, L.Z. Zhu, Influences of
483 installation and tracking errors on the optical performance of a solar parabolic
484 trough collector, Renewable Energy 94 (2016) 197-212.
485 [46] C.Z. Zhang, G.Q Xu, Y.K. Quan, H.W. Li, G. Song, Optical sensitivity analysis
486 of geometrical deformation on the parabolic trough solar collector with Monte
487 Carlo Ray-Trace method, Applied Thermal Engineering 109 (2016) 130-137.
488 [47] J.F. Song, Z.L. Zhou, K. Tong, An algorithm for the flux distribution over the flat
489 absorber of a parabolic trough concentrator, Solar Energy 125 (2016) 32-42.
490 [48] J.F. Song, K. Tong, L. Li, G. Luo, L.J. Yang, J. Zhao, A tool for fast flux
491 distribution calculation of parabolic trough solar concentrators, Solar Energy 173
492 (2018) 291-303.
493 [49] H.B. Liang, S.J. You, H. Zhang, Comparison of three optical models and analysis
494 of geometric parameters for parabolic trough solar collectors, Energy 96 (2016)
495 37-47.

[50] H.B. Liang, M. Fan, S.J. You, W.D. Zhang, H. Zhang, T.Z. Ye, et al. A Monte Carlo method and finite volume method coupled optical simulation method for parabolic trough solar collectors, Applied Energy 201 (2017) 60-68.

[51] J.J. Serrano-Aguilera, L. Valenzuela, J. Fernandez-Reche, Inverse Monte Carlo Ray-Tracing method (IMCRT) applied to line-focus reflectors, Solar Energy 124 (2016) 184-197.

[52] J.J. Serrano-Aguilera, L. Valenzuela, J. Fernandez-Reche, Modified geometry of line-focus collectors with round absorbers by means of the inverse MCRT method, Solar Energy 139 (2016) 608-621.

[53] A. Mwesigye, Z.J. Huan, T. Bello-Ochende, J.P. Meyer, Influence of optical errors on the thermal and thermodynamic performance of a solar parabolic trough receiver, Solar Energy 135 (2016) 703-718.

[54] J. Sun, R.L. Wang, H. Hong, Q.B. Liu, An optimized tracking strategy for small-scale double-axis parabolic trough collector, Applied Thermal Engineering 112 (2017) 1408-1420.

[55] J.F. Song, K. Tong, G. Luo, L. Li, Influence of non-ideal optical factors in actual engineering on the safety and stability of a parabolic trough collector, Renewable Energy 113 (2017) 1293-1301.

[56] B. Zou, J.K. Dong, Y. Yao, Y.Q. Jiang, A detailed study on the optical performance of parabolic trough solar collectors with Monte Carlo Ray Tracing method based on theoretical analysis, Solar Energy 147 (2017) 189-201.

517 [57] H. Hoseinzadeha, A. Kasaeianb , M.B. Shafii, Geometric optimization of
518 parabolic trough solar collector based on the local concentration ratio using the
519 Monte Carlo method, Energy Conversion and Management 175 (2018) 278-287.
520 [58] Z.D. Cheng, X.R. Zhao, Y.L. He, Novel optical efficiency formulas for parabolic
521 trough solar collectors: computing method and applications, Applied Energy 224
522 (2018) 682-697.
523 [59] M. Fan, S.J. Youa, J.B. Xia, W.D. Zheng, H. Zhanga, H.B. Liang, et al., An
524 optimized Monte Carlo ray tracing optical simulation model and its applications to
525 line-focus concentrating solar collectors, Applied Energy 225 (2018) 769-781.
526 [60] B. Zou, Y. Yao, Y.Q. Jiang, H.X. Yang, A new algorithm for obtaining the critical
527 tube diameter and intercept factor of parabolic trough solar collectors, Energy 150
528 (2018) 451-467.
529 [61] I.H. Yilmaza, A. Mwesigye, Modeling, simulation and performance analysis of
530 parabolic trough solar collectors: A comprehensive review, Applied Energy 225
531 (2018) 135-174.
532 [62] E. Bellos, C. Tzivanidis, Alternative designs of parabolic trough solar collectors,
533 Progress in Energy and Combustion Science 71 (2019) 81-117.
534 [63] G.K. Manikandana, S. Iniyanb, R. Goic, Enhancing the optical and thermal
535 efficiency of a parabolic trough collector-A review, Applied Energy 235 (2019)
536 1524-1540.
537 [64] E. Bellos, C. Tzivanidis, Investigation of a booster secondary reflector for a

parabolic trough solar collector, Solar Energy 179 (2019) 174-185.

[65] D. Buie, A.G. Monger, C.J. Dey, Sunshape distributions for terrestrial solar simulations, Solar Energy 74 (2003) 113-122.

[66] Neumann A, Schubnell M. Irradiance and sunshape measurements for the Cologne site, In: Proceedings of the 8th International Solar Forum, 1992, pp. 1173-1183.

[67] Neumann A, Witzke A, Jones SA, Schmitt G. Representative terrestrial solar brightness profiles, Journal of Solar Energy Engineering 2002; 124: 198-204.

[68] R.B. Pettit, Characterization of the reflected beam profile of solar mirror materials, Solar Energy 19 (1977) 733-741.

[69] R.B. Pettit, C.N. Vittitoe, F. Biggs, Simplified calculational procedure for determining the amount of intercepted sunlight in an imaging solar concentrator, Journal of Solar Energy Engineering 105 (1983) 101-107.

[70] G. Johnston, On the analysis of surface error distributions on concentrated solar collectors, ASME Journal of Solar Energy Engineering 117 (1995) 294-296.

[71] V.E. Dudley, G. Kolb, M. Sloan, D. Kearney, Test results: SEGS LS2 Solar Collector, Report of Sandia National Laboratories, Albuquerque, 1994, NM SANDIA 94-1884.

Figure:

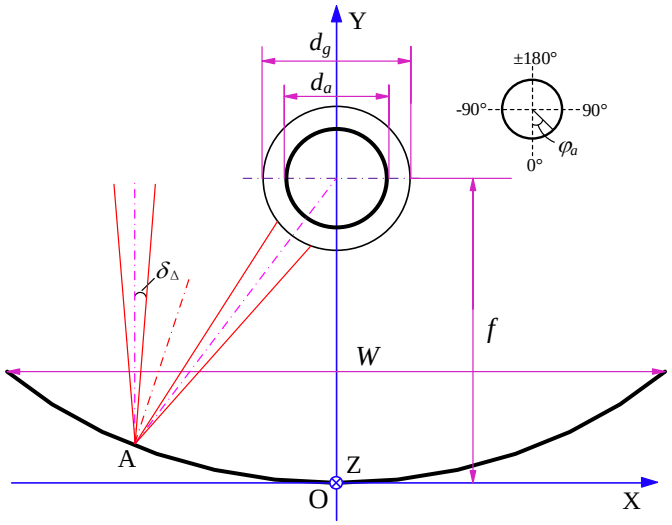

Fig. 1 Schematic diagram of the cross section of a PTC module

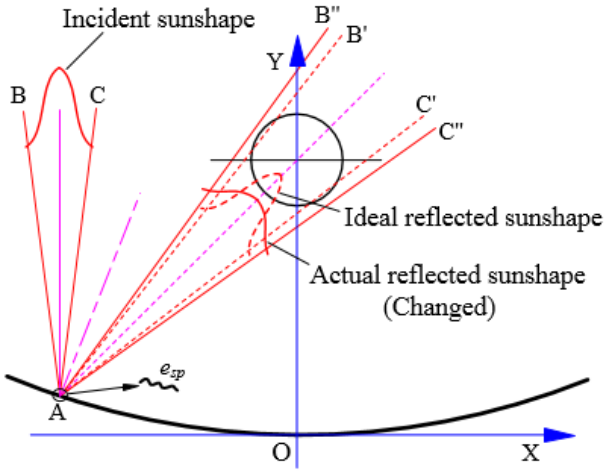

Fig. 2 Effect of specularity error on the reflected sunshape

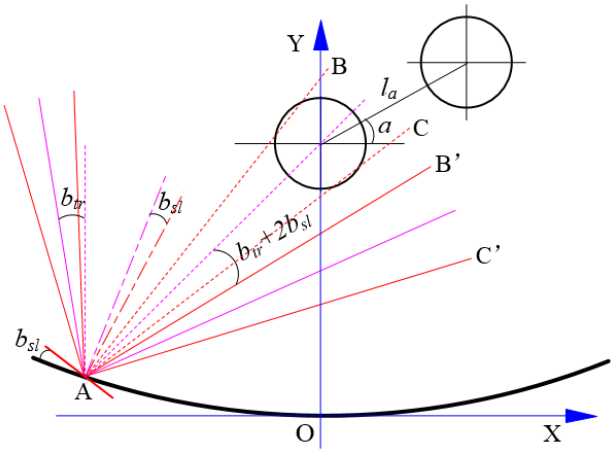

Fig. 3 Geometric description of optical errors

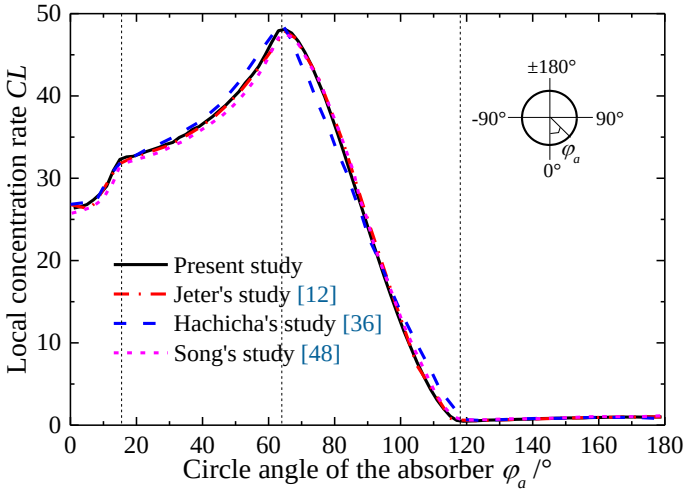

Fig. 4 Comparison of local concentration ratio distribution obtained by different methods

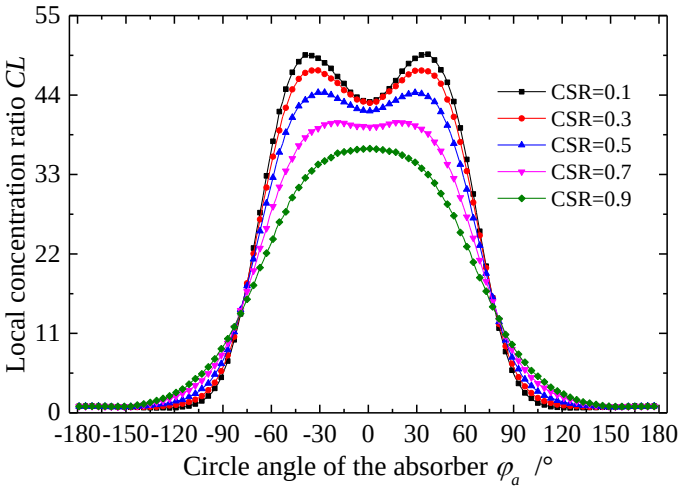

578

579 Fig. 5 Effects of circumsolar ratio (CSR) on the distribution of local

580 concentration ratio (*CL*) in the case of σ_{sp}=3 mrad

581

582

583

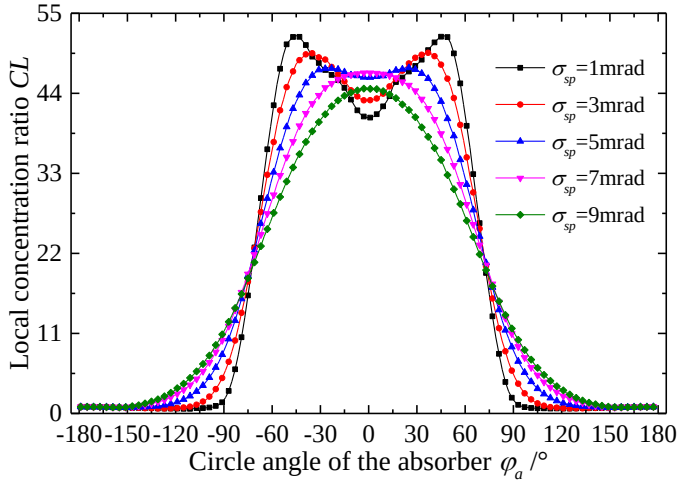

584

585 Fig. 6 Effects of specularity error (σ_{sp}) on the distribution of local concentration

586 ratio (*CL*) in the case of CSR=0.1

587

588

589

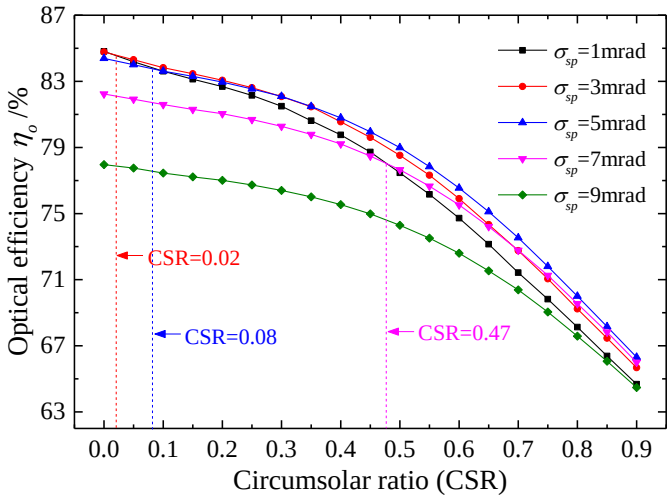

590

591 Fig. 7 Variation of the optical efficiency (η_o) with circumsolar ratio (CSR) under

592 different specularity errors (σ_{sp})

593

594

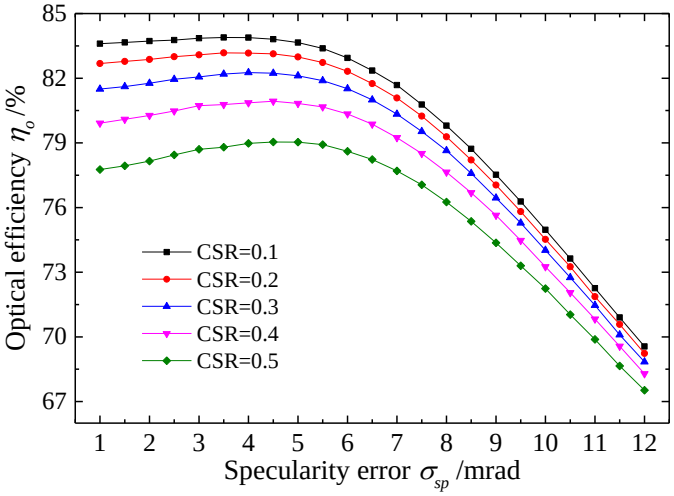

595

596 Fig. 8 Variation of the optical efficiency (η_o) with specularity error (σ_{sp}) under

597 different circumsolar ratios (CSR)

598

599

600

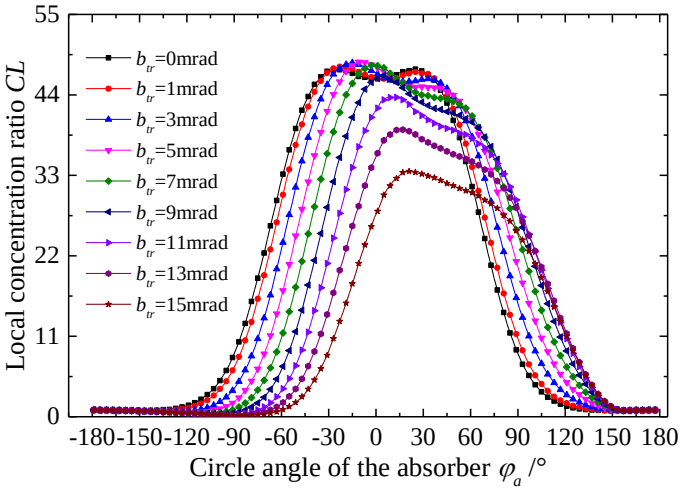

601

602 Fig. 9 Effects of tracking error (b_{tr}) on the distribution of local concentration

603 ratio (*CL*)

604

605

606

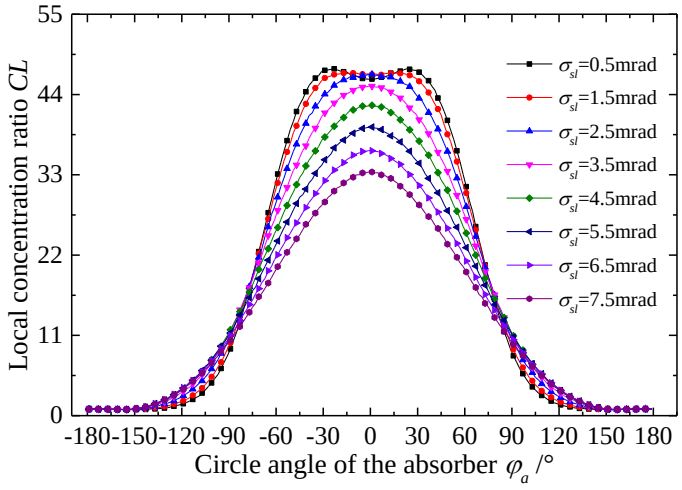

607

608 Fig. 10 Effects of slope error (σ_{sl}) on the distribution of local concentration ratio

609 (*CL*)

610

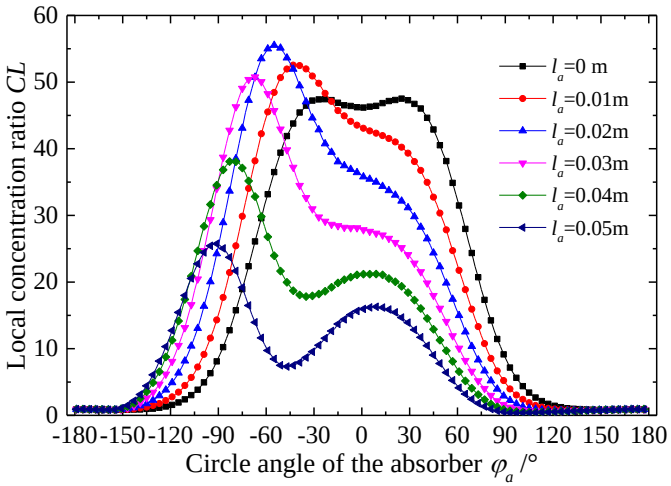

611

612 (a)

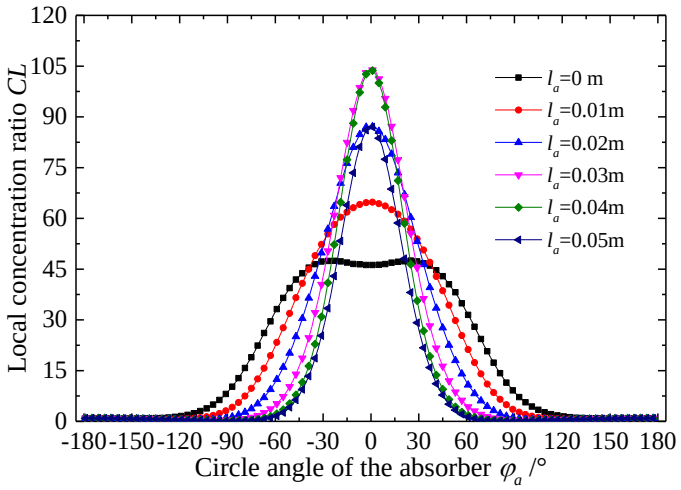

613

614 (b)

615 Fig. 11 Effects of the absorber alignment error on the distribution of local

616 concentration ratio (*CL*): (a) a =0°, (b) a =90°

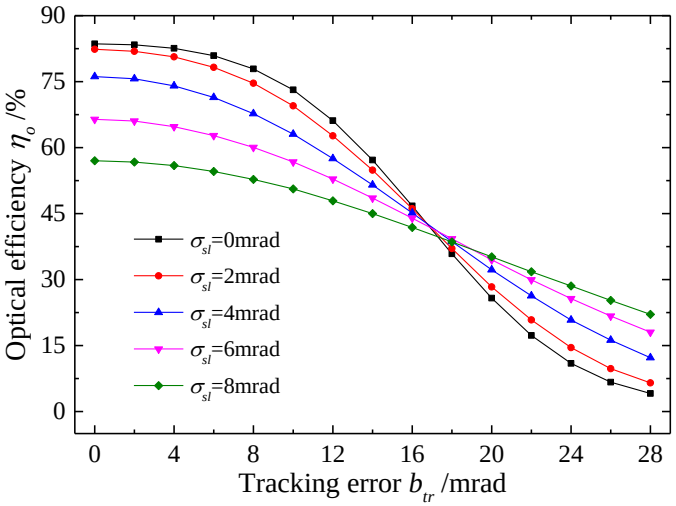

617

618 Fig.12 Variation of the optical efficiency (η_o) with tracking error (b_{tr}) under

619 different slope errors (σ_{sl})

620

621

622

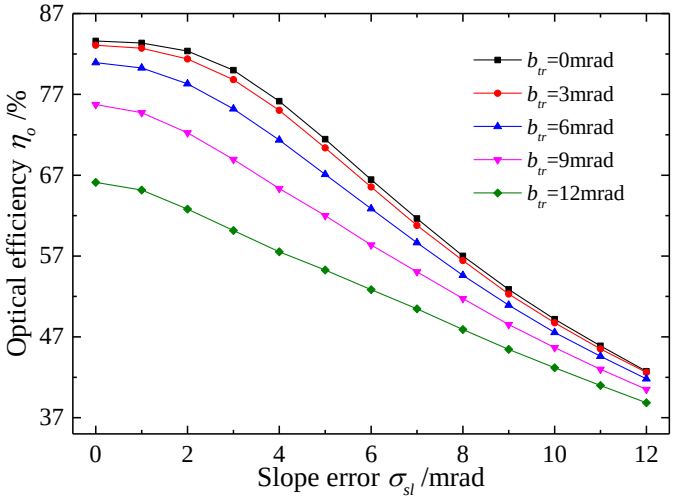

623

624 Fig. 13 Variation of the optical efficiency (η_o) with slope error (σ_{sl}) under

625 different tracking errors (b_{tr})

626

627

628

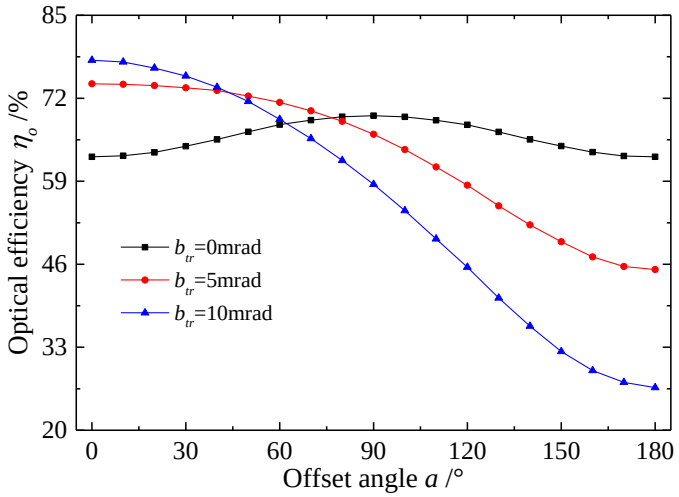

629

630 Fig. 14 Variation of the optical efficiency (η_o) with offset angle (a) for l_a =0.03

631 m under different tracking errors (b_{tr}) in the case of σ_{sl} =3 mrad

632

633

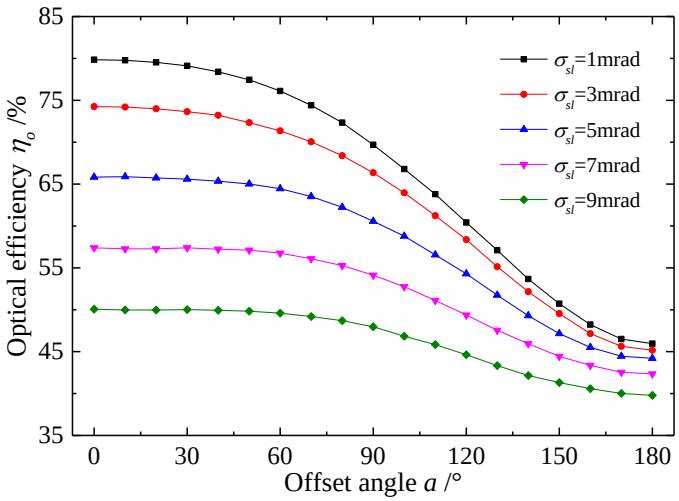

634

635 Fig. 15 Variation of the optical efficiency (η_o) with offset angle (a) for l_a

636 =0.03m under different slope errors (σ_{sl}) in the case of b_{tr} =5 mrad

637

638

639 Table 2 Parameters of SEGS LS-2 PTC module [71]

Parameter	Value	Unit
W	5	m
f	1.84	m
L_a	7.8	m
d_a	0.07	m
d_g	0.115	m
α_a	0.96	——
ρ_r	0.93	——
τ_g	0.95	——

640